Journal of Porous Materials (2020) 27:1265–1275
https://doi.org/10.1007/s10934-020-00898-w

In-situ synthesis of hierarchical lamellar ZSM-5 zeolite with enhanced MTP catalytic performance by a facile seed-assisted method

Yan-Hong Chen[1] · Dong-Min Han[1] · Qiang Zhang[2] · Hong-Xia Cui[1]

Published online: 23 May 2020

Abstract
A seed-assisted route has been applied to prepare the hierarchical lamellar ZSM-5 zeolite with good porosity and catalytic performance in methanol to propylene (MTP) reaction. In this method, ZSM-5 crystal seeds instead of organic quaternary ammonium were used to direct the formation of ZSM-5 nuclei and conventional surfactant cetyltrimethylammonium bromide (CTAB) employed as the mesoporogen. The process for the formation of hierarchical lamellar ZSM-5, including the effect of the ratio of CTAB/SiO_2, initial gel aging temperature, synthesis temperature and synthesis time were discussed in detail. The results suggested that mesoporous structure was first obtained and then transformed into MFI structure in-situ during the hydrothermal synthesis process. The obtained hierarchical lamellar ZSM-5 zeolite displays an organized flack-like nanosheet stacks morphology with regular intercrystal mesopores of 3–7 nm, possessing large surface area and mesopore volume. Moreover, the synthesized hierarchical ZSM-5 zeolite has perfect catalyst lifetime in methanol to propylene (MTP) reaction than conventional microporous ZSM-5 zeolite, which could be ascribed to the hierarchical mesoporous structure accommodating more bulky molecules and accessible acid sites in the catalytic reaction.

Keywords Hierarchical ZSM-5 · CTAB · Seeds · Nanosheets

1 Introduction

Zeolites with well-defined pores have been extensively used in the fields of petroleum and petrochemistry for its shape selectivity, high acidity and good thermal/hydrothermal stability [1–3]. However, the dimensions of micropores limit the diffusion rate of large molecules, which leaves a large part of acid sites within a zeolite crystals can not be utilized leading to the low catalytic efficiencies and undesired secondary reactions such as coke deposition. In order to solve these problems, a lot of measures have been made, such as the synthesis of nanozeolites and ordered mesoporous materials [4–6]. A variety of synthetic methods for the preparation of nanozeolites have been reported in recent years. The reduced crystal size of zeolite nanocrystals can increase the external surface area and reduce the diffusion path, thus improving the catalytic activity [7]. But the difficulty of separation nanozeolites from the reaction mixture and low yields in synthesis would hinder their practical applications. The relative low hydrothermal and catalytic activity of ordered mesoporous materials are also unfavorable for practical catalytic reactions [8]. Hierarchical zeolites are materials with improved transport rate and coke resistance in which mesopores are integrated in crystalline microporous zeolites. Therefore, hierarchical zeolites are regarded as the best strategy and have been paid great attention in recent years [9–12]. Generally, the additional porosity can be introduced within or between zeolite crystals via post treatments (including steaming dealumination, acid dealumination and base desilication) and indirect templating methods (including hard templating methods and soft templating methods) [13–18]. However, the major drawback to

Electronic supplementary material The online version of this article (https://doi.org/10.1007/s10934-020-00898-w) contains supplementary material, which is available to authorized users.

✉ Yan-Hong Chen
chenning995@163.com

✉ Qiang Zhang
xyz@upc.edu.cn

[1] Department of Chemical Engineering, Shengli College China University of Petroleum, Dongying 257100, Shandong Province, China

[2] State Key Laboratory of Heavy Oil Processing, China University of Petroleum, Qingdao 266580, Shandong Province, China

post treatments is the inability to control mesopores formation and the loss of crystallinity. Although, hard templating methods with carbon could produce oriented, straight mesopores, abundant of carbon used in many synthesis processes hinders industrial application. The soft-templating method, including cationic surfactants, silylated polymer and amphiphilic organo-silane, has been paid increasing attention for its facile production. In addition, uniform and ordered mesoporous zeolite can be synthesized through the self-assembly process which avoid separate growth of microporous and mesoporous materials.

ZSM-5 with 10-ring micropores is one of the most widely studied and commonly used zeolites which has exhibited excellent catalytic properties in many fields such as cracking, isomerization, alkylation and aromatization. Thus, great interest has been generated in the synthesis of hierarchical ZSM-5 [15–21]. Rayoo's group synthesized MFI zeolite nanosheets possessing uniform mesopores by using designed diquaternary ammonium surfactant as template [20]. Recently, single-crystalline MFI nanosheets were prepared using a new design of amphiphilic molecules with aromatic-group tail as template. It is the result of π–π interaction of aromatic groups in amphiphilic molecules directing for single-crystalline mesostructured zeolite nanosheets [21, 22]. Compared with those of other mesoporous and conventional MFI zeolites, the nanosheet morphology along with the high external surface area and reduced crystal thickness accounts for higher reaction rates for bulky molecules and thereby dramatically suppresses catalyst deactivation through coke deposition. The large number of acid sites on the external surface of these zeolites renders them highly active for the catalytic conversion of large organic molecules as well. However, the templates used in these methods are too expensive to the wide applications in industry. Traditional cationic surfactant cetyltrimethylammonium bromide (CTAB) as a soft template to prepare hierarchical zeolites has attracted people's attention since the discovery of MCM series. CTAB as mesoporogen is low cost and little environmental impact. However, it usually has a competition between CTAB self-assemble and the structure-direction agent (SDA) leading to physical mixtures of bulk ZSM-5 and MCM-41 [23, 24]. To solve the phase separation, a seed-induced method is an effective way in which CTAB as a mesopore-directing agent template interacted with the pre-crystallized precursor seed subnanocrystals to synthesis hierarchical ZSM-5 [25–29]. In general, precrystallization of the zeolite precursor played key roles in producing a large number of subnanocrystal-type zeolite seeds, which has relatively high polymerization degrees. Nevertheless, a large number of TPAOH were unavoidable as zeolite-forming SDA in these methods. In addition, most hierarchical ZSM-5 zeolites reported using CTAB as soft template are sphere-like [28–30].

In this work, lamellar ZSM-5 zeolite nanosheets were green prepared by a facile, low cost seed-assisted synthesis strategy with CTAB as the only organic template. Zeolite seeds replaced TPAOH by adding synthesis gel for directing the formation of ZSM-5 structure which effectively avoided the phase separation caused by competition with CTAB. The influence of the amount of CTAB, aging temperature, synthesis temperature, synthesis time on crystallinity, morphology and physicochemical properties were investigated in detail. The synthesized hierarchical ZSM-5 zeolite displays large external surface area, mesopore volume and narrow intercrystal mesopore. The catalytic performance of the obtained hierarchical ZSM-5 zeolite was evaluated in methanol to propylene (MTP) reaction, which exhibits greatly improved catalyst lifetime and propylene selectivity compared with conventional ZSM-5 zeolite.

2 Experimental

2.1 Reactants

The following chemical reactants were used: aluminum sulfate octadecahydrate ($Al_2(SO_4)_3{\cdot}18H_2O$, 99.0 wt%), water glass (SiO_2 = 28 wt%, Na_2O = 9 wt%), CTAB (AR, 99.0 wt%), sulphuric acid (H_2SO_4 AR, 98%), ZSM-5 seeds (SiO_2/Al_2O_3 = 50, obtained from Tianjin Guangfu Chemical Reagent Co., China. The XRD pattern and SEM image of ZSM-5 seeds are shown Fig. S1), deionized water (H_2O).

2.2 Synthesis of the hierarchical ZSM-5

The hierarchical ZSM-5 (Hi-ZSM-5) were prepared as follows. At first, 1.16 g of aluminum sulfate octadecahydrate was dissolved in 35 g of deionized water and stirred at room temperature. Then 25 g of water glass was added dropwise into the stirring solution. In order to adjust Na_2O/SiO_2 ratio of synthesis system, 1.5 g of H_2SO_4 was dropped to neutralize excessive alkali ingredients in water glass system under continuous stirring condition to obtain a homogeneous aluminosilicate gel, then 0.5 g of ZSM-5 seeds were added into the gel and stirred for 1 h. The gel mixture was left at 60 °C, 24 h for aging. After aging, the resulting hydrogel mixture was introduced 5.5 g of CTAB to obtain a mixture with molar composition of $60SiO_2{:}1Al_2O_3{:}4Na_2O{:}6CTAB{:}2400H_2O$. After stirring for 2 h at room temperature, the gel was hydrothermally treated at 150 °C for different time. The solid product was filtered, washed, dried and finally calcined in air at 550 °C for 6 h.

For comparison, a conventional ZSM-5(C-ZSM-5) obtained at 150 °C, 4 days with molar composition of $60SiO_2:1Al_2O_3:4Na_2O:2400H_2O$ and seed crystals (5 wt% based on total silica amount) was employed as a reference.

2.3 Characterization

X-ray diffraction (XRD) was recorded on a Rigaku X'Pert PRO MPD diffractometer with Cu *Kα* radiation (45 kV and 40 mA). Scanning electron microscopy (SEM) was performed with a JSM-7800F field emission scanning electron microscope operating at 3 kV. High-resolution TEM (HR-TEM) pictures were obtained on a JEM 2100F microscope instrument at 200 kV. The N_2 adsorption and desorption isotherms were measured using a QuantaChrome Autosorb-iQ porosity analyze at 77 K. The NH_3-TPD profiles were taken on a Micrometitics Tianjin Xianquan, TP-5079 chemical adsorption instrument.

2.4 Catalytic tests

All of the samples used in catalytic tests were H-form. The MTP reaction was conducted in a micro-activity test (MAT) unit at 400 °C under atmospheric pressure. For a typical run, 0.5 g catalyst (20–60 mesh) was placed in the fixed bed reactor with an internal diameter of 10 mm. After temperature increased stable to 400 °C, then the liquid methanol was pumped into the reactor with nitrogen as the carrier gas, at a weight hourly space velocity (WHSV) of 10 h^{-1}. The gaseous products were analyzed on a Shanghai GC9310 Chromatograph fitted with TCD and FID detectors. The corresponding liquid hydrocarbons were analyzed on Beijing PERSEE G5 gas chromatograph with an KB-5 capillary column (50 m × 0.32 mm × 0.25 μm). The methanol conversion and propylene selectivity were defined as follows:

$$Methanol\ conversion\ (\%) = \left(M_{in} - M_{out} - 2M_{DME}\right)/M_{in} \times 100\%$$

where M_{in}, M_{out} and M_{DME} denoted the amounts of pumped in, unconverted methanol, and the produced dimethylether, respectively.

$$Propylene\ selectivity\ (\%) = M_p/M_{HC} \times 100\%$$

where M_p was the amount of the propylene to be calculated and M_{HC} was the total amount of hydrocarbon products.

3 Results and discussion

3.1 Characterization of Hi-ZSM-5 zeolites

In order to study the effect of the CTAB content on crystal morphology, crystal phase and textural properties of the Hi-ZSM-5 zeolites, samples synthesized with different contents of CTAB were characterized by XRD, SEM, TEM and N_2 adsorption and desorption, in comparison with C-ZSM-5. The initial gel molar composition was $60SiO_2:1Al_2O_3:4Na_2O:xCTAB:2400H_2O$ with x being 0.05, 0.1 or 0.2 and the prepared samples were designated as MZ-x, in which x represents the molar ratio of CTAB to SiO_2. The steps of crystallization were accomplished at 150 °C for 4 days. The high and low-angle XRD patterns of the as-synthesized samples are shown in Fig. 1. When

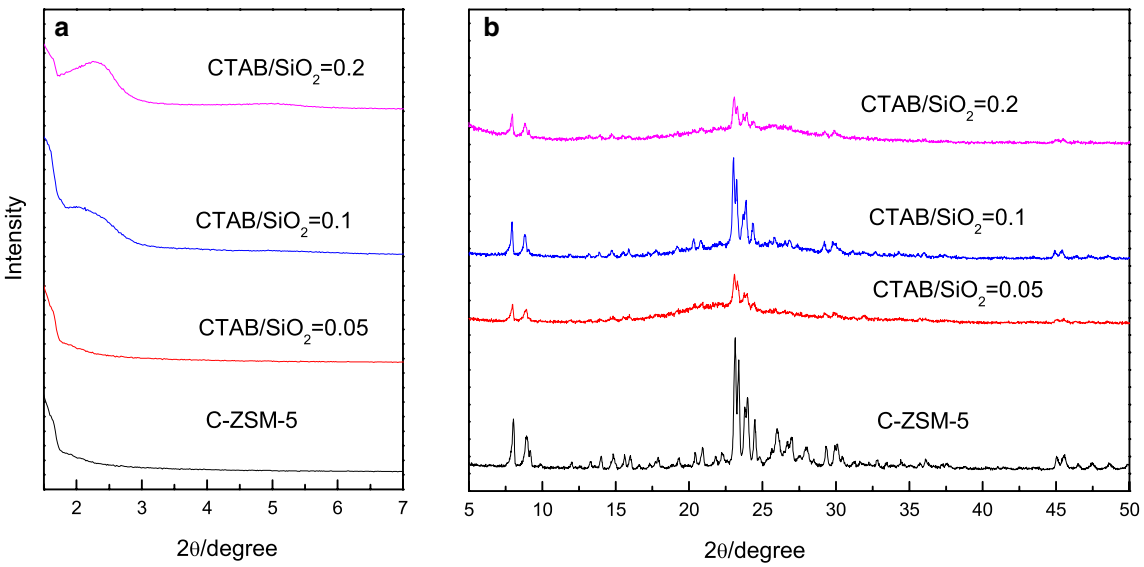

Fig. 1 Low-angle and wide-angle XRD patterns of Hi-ZSM-5 with different ratios of CTAB/SiO_2: 0, 0.05, 0.1 and 0.2

different contents of CTAB were introduced to the synthesis system ($CTAB/SiO_2 = 0.05$, 0.1 and 0.2, respectively), as shown in Fig. 1, the $CTAB/SiO_2$ ratios were critical for Hi-ZSM-5 synthesis. In the low-angle XRD region (Fig. 1a), there is no peak at low ratio of $CTAB/SiO_2$ of 0.05, implying that too little CTAB to form ordered mesopores. With the increase of $CTAB/SiO_2$ ratios from 0.05 to 0.2, a single peak can be observed and strengthens gradually which can be ascribed to the low-order secondary structuring at the mesoscale demonstrating the lamellar structural feature. The low-angle reflection peaks disappear in the corresponding calcined lamellar Hi-ZSM-5 (Fig. S2), which was caused by the collapse of zeolite layer during the process of surfactant template removal. Simultaneously, in the wide-angle part of the XRD region (Fig. 1b), it shows that the obtained sample is poorly crystallized at low ratio of $CTAB/SiO_2$ of 0.05. With increasing the $CTAB/SiO_2$ to 0.1, the sample of MZ-0.1 exhibits a typical MFI-type topology of zeolite ZSM-5 with peaks at 2θ of 7.9, 8.7, 23.1 23.9 and 24.4. The relative crystallinity of MZ-0.1 is slightly lower than that of C-ZSM-5 used as the reference sample, which is due to the formation of smaller nanosheet crystallites and then assembled to form the intercrystalline mesopores. When the ratio of $CTAB/SiO_2$ is further increased to 0.2, the double peaks between 7° and 10° and the triple peaks between 22° and 25° ascribing to the MFI topology of resulting material decreases dramatically. The result indicates that an excessive ratio of ratio of $CTAB/SiO_2$ with hydrophobic carbon chains inhibited the nucleation and growth of the zeolite.

The N_2 sorption isotherms and the relevant BJH pore size distribution of all MZ-x samples are presented in Fig. 2. Obviously, the C-ZSM-5 exhibits only a steep increase in the curve at very low relative pressure (near $P/P_0 = 0$), almost without an adsorption hysteresis loop, which is consistent with the typical nitrogen adsorption type I isotherm of microporous material. The corresponding BJH pore size distribution further indicates that there is no mesopores. In the case of the samples synthesized with CTAB, the nitrogen adsorption behavior is dramatically different from that of C-ZSM-5. In fact, N_2 sorption isotherms for MZ-0.1 and MZ-0.2 both show a composite of type I and IV isotherm with a hysteresis loop and enhanced uptake at higher P/P_0, indicating the materials with the composited structure of both micropores and mesopores (Fig. 2a). The shape of the hysteresis loop shows a type H3 indicative of slit-like mesopores. The corresponding BJH pore size distribution with the mesopore sizes in the range of 3–7 nm with the peak at around 3.8 nm and 5 nm respectively further confirmed presence of mesoporosity (Fig. 2b). However, the type I isotherm remains in the sample synthesized with a $CTAB/SiO_2$ ratio of 0.05 indicating that there is no formation of mesopores and a small adsorption capacity is found, which is due to the low crystallinity in this sample. The result is also confirmed by the XRD characterization. The poor physicochemical properties of MZ-0.05 were observed, as shown in Table 1.

Textural properties of all MZ-x samples are reported in Table 1. It shows that both the samples of MZ-0.1 and MZ-0.2 possess largely improved external surface area ($S_{ex} = 287\ m^2\ g^{-1}$ and $353\ m^2\ g^{-1}$, respectively) and mesopore volume ($V_{meso} = 0.37\ cm^3\ g^{-1}$ and $0.55\ cm^3\ g^{-1}$, respectively). It is clearly higher than that of C-ZSM-5

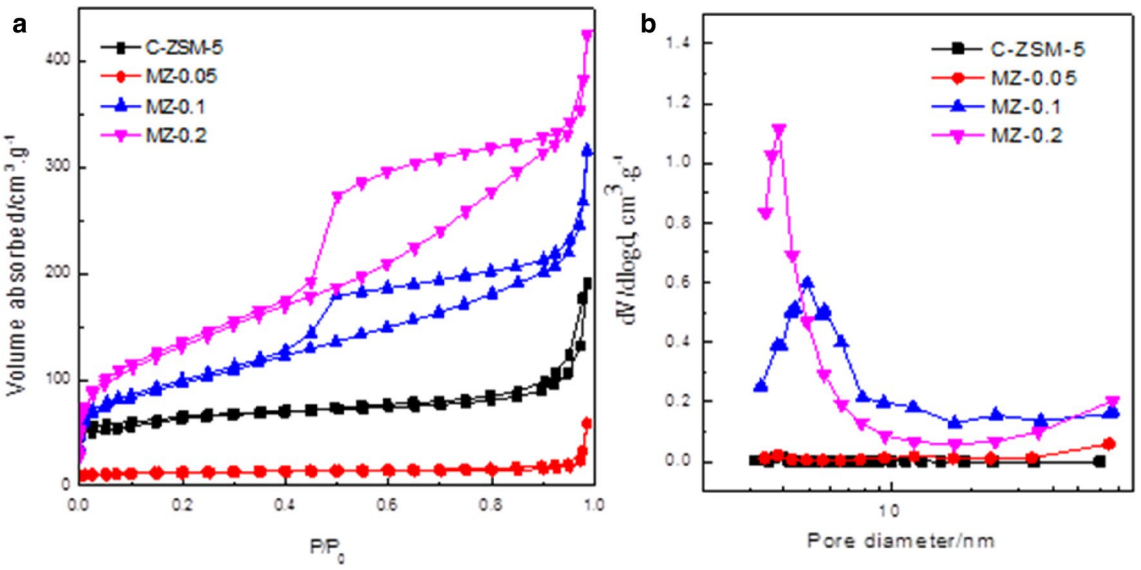

Fig. 2 N_2 adsorption/desorption isotherms and corresponding BJH pore size distribution of of Hi-ZSM-5 with different ratios of $CTAB/SiO_2$: 0, 0.05, 0.1 and 0.2

Table 1 Textural parameters of Hi-ZSM-5 and C-ZSM-5

Sample	Specific surface area ($m^2\ g^{-1}$)			Pore volume ($cm^3\ g^{-1}$)		
	S_{BET}[a]	S_{micro}[b]	S_{ex}[c]	V_{tot}[d]	V_{micro}[e]	V_{meso}[f]
MZ-0.05	45	39	6	0.08	0.013	0.067
MZ-0.1	444	157	287	0.45	0.08	0.37
MZ-0.2	425	72	353	0.58	0.03	0.55
C-ZSM-5	248	222	26	0.16	0.09	0.07

[a]S_{BET} determined by the BET method

[b]Calculated using t-plot method

[c]$S_{ex} = S_{BET} - S_{micro}$

[d]Obtained from the amount adsorbed at $p/p_0 = 0.995$

[e]Calculated using t-plot method

[f]$V_{meso} = V_{total} - V_{micro}$

(26 $m^2\ g^{-1}$ and 0.07 $cm^3\ g^{-1}$, respectively), which suggest mesoporous properties development. The samples with large mesopore volume can not only supply them with a large portion of external active sites but also easy access to the active acid sites in micropores, which are important to catalytic reaction. The micropore surface area ($S_{micro} = 157$ $m^2\ g^{-1}$) and micropore volume ($V_{micro} = 0.08$ $cm^3\ g^{-1}$) of sample MZ-0.1 are comparable to that of C-ZSM-5 (222 $m^2\ g^{-1}$ and 0.09 $cm^3\ g^{-1}$, respectively), revealing formation abundant of mesopores during the synthesis process while retaining the micropore structure. Hierarchy factor (HF) is a quantitative tool to demonstrate the hierarchical pore structure of samples, which is defined as the product of (V_{micro}/V_{pore}) × (S_{meso}/S_{BET}). MZ-0.1 shows a higher HF (0.12) compared with that of the C-ZSM-5 (0.06), indicating hierarchical porous character. However, MZ-0.2 has a relative lower S_{micro} (72 $m^2\ g^{-1}$) and V_{micro} (0.03 $m^2\ g^{-1}$). It is well accordance with the XRD pattern results where the crystallinity of MZ-0.2 is also smaller than MZ-0.1 (Fig. 1b). Therefore, the optimal of CTAB/SiO_2 ratio is 0.1 to synthesis highly crystalline Hi-ZSM-5 zeolite in this work, further characterization and catalytic reactions were tested using the sample MZ-0.1 as well. All of the above results indicate that CTAB plays an important role in the meso-structure assembly process with subnanocrystals and a medium level of CTAB is needed. The meso- and microporosity of samples can be tuned by changing the amount of CTAB. The formation of Hi-ZSM-5 was a result of self-assembly between the subnanocrytal zeolite seeds and CTAB.

The SEM and HR-TEM were employed to characterize the morphologies and the mesopores structure of the samples. The morphologies of samples prepared with or without CTAB are significantly different. The C-ZSM-5 zeolite synthesized in the absence of CTAB displays large hexagonal-shaped crystals with size about 2 µm (Fig. 3a). With the use of CTAB in the synthesis of ZSM-5, a remarkable change in the morphology of the crystal was observed which indicated that the presence of CTAB affects the crystal growth process. The SEM images clearly show that the sample MZ-0.05 consists of bulky irregular particles with mostly amorphous gel (Fig. 3b), while the other two samples (Fig. 3d, f) have crystallized flake-like particle aggregates which correlates well with the results of previous discussions. Consequently it can be concluded that the little CTAB not only failed to form mesoporous structure, but also destroyed the stable synthesis system of ZSM-5 zeolite. With the increase of CTAB/SiO_2 to 0.1, the MZ-0.1 displays honeycomb morphology (Fig. 3c), in which numerous flake-like crystals stack loosely (Fig. 3d). As a result, the intercrystalline mesopores are formed among these aggregated flake-like crystals. Increasing the CTAB/SiO_2 to 0.2, the nanosheet stacks change to a more organized structure and obvious amorphous phase is observed (Fig. 3e, f), The presence of mesopores in the Hi-ZSM-5 can be further confirmed from HR-TEM images. It reveals that a solid dense particle indicating low transmission of the electron beam is seen in C-ZSM-5 implying no evident mesopores in the sample (Fig. 3g). However, numerous nanosheet crystals stacking along the same orientation loosely together can be obviously observed in the sample of MZ-0.1 (Fig. 3h, i). In such cases, the mesopores between each nanosheet crystals are formed.

These analyses further proved mesoporous structure appears in Hi-ZSM-5 with assistance of CTAB. The large external surface area and supplementary mesopores would enhance the accessibility and molecular diffusion rate which affect stability and selectivity of zeolite. The Hi-ZSM-5 zeolite is believed to be great beneficial in catalytic reaction dealing with bulky intermediates and/or products.

3.2 Synthesis of Hi-ZSM-5 zeolites

A number of factors were essential for the formation of Hi-ZSM-5, including the aging temperature, crystallization temperature and crystallization time. Three series of Hi-ZSM-5 samples were prepared at different aging temperature 40 °C, 60 °C and 80 °C for 24 h,

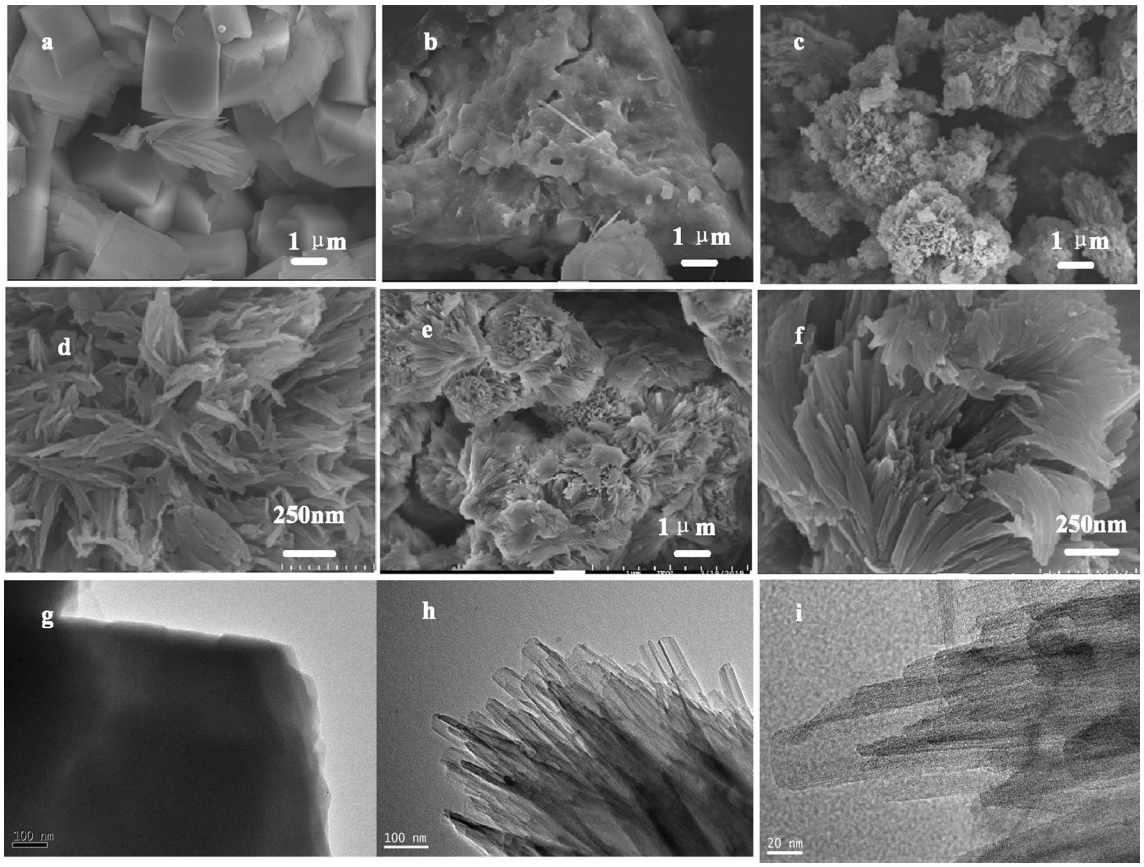

Fig. 3 SEM images and HR-TEM images of C-ZSM-5 (**a**, **g**) and Hi-ZSM-5 with different ratios of CTAB/SiO_2: 0.05 (**b**), 0.1 (**c**, **d**, **h**, **i**) and 0.2 (**e**, **f**)

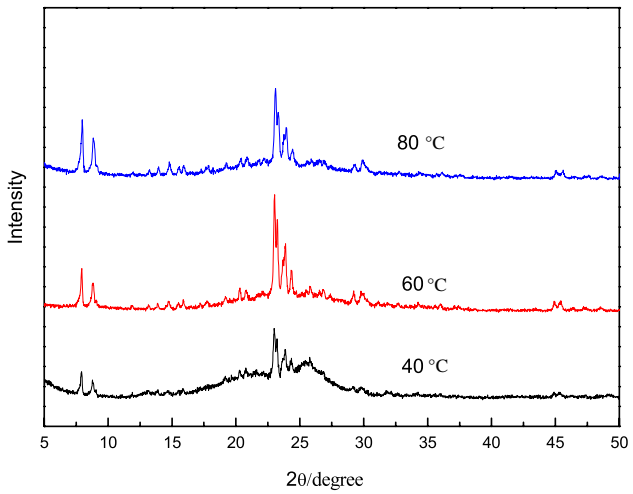

Fig. 4 XRD patterns of Hi-ZSM-5 synthesized with aging temperature of 40 °C, 60 °C and 80 °C

respectively. The initial gel compositions of all samples were $60SiO_2$:$1Al_2O_3$:$4Na_2O$:6CTAB:$2400H_2O$ with 0.5 wt% of the ZSM-5 seed crystals. The XRD patterns of Hi-ZSM-5 synthesized at different aging temperature are shown in Fig. 4. It shows that at the low aging temperature 40 °C, the crystallinity of ZSM-5 is poor, which indicates that the zeolite precursor contains too higher amount of less polymerized silica to formation ZSM-5 crystals at a lower aging temperature. The increase of the aging temperature from 40 to 60 °C enhances the ZSM-5 crystallinity. However, a further increase of the aging temperature to 80 °C, the crystallinity of ZSM-5 no longer increases, which shows that a mild aging temperature at 60 °C is sufficient to induce the formation of higher polymerization degrees of subnanocrystal.

It is recognized that the synthesis temperature is an important parameter in the zeolite synthesis. Effect of crystallization temperature on synthesis of Hi-ZSM-5 was studied by running three experiments at different crystallization temperature for 4 days (120 °C, 150 °C, and 180 °C, respectively). Figure 5 shows the XRD patterns and the SEM images of the samples synthesized at different crystallization temperature. At the lowest crystallization temperature 120 °C, an amorphous material with little ZSM-5 crystals was obtained, according to the low intensity of the XRD patterns (Fig. 5a) and lamellar-like morphologies in

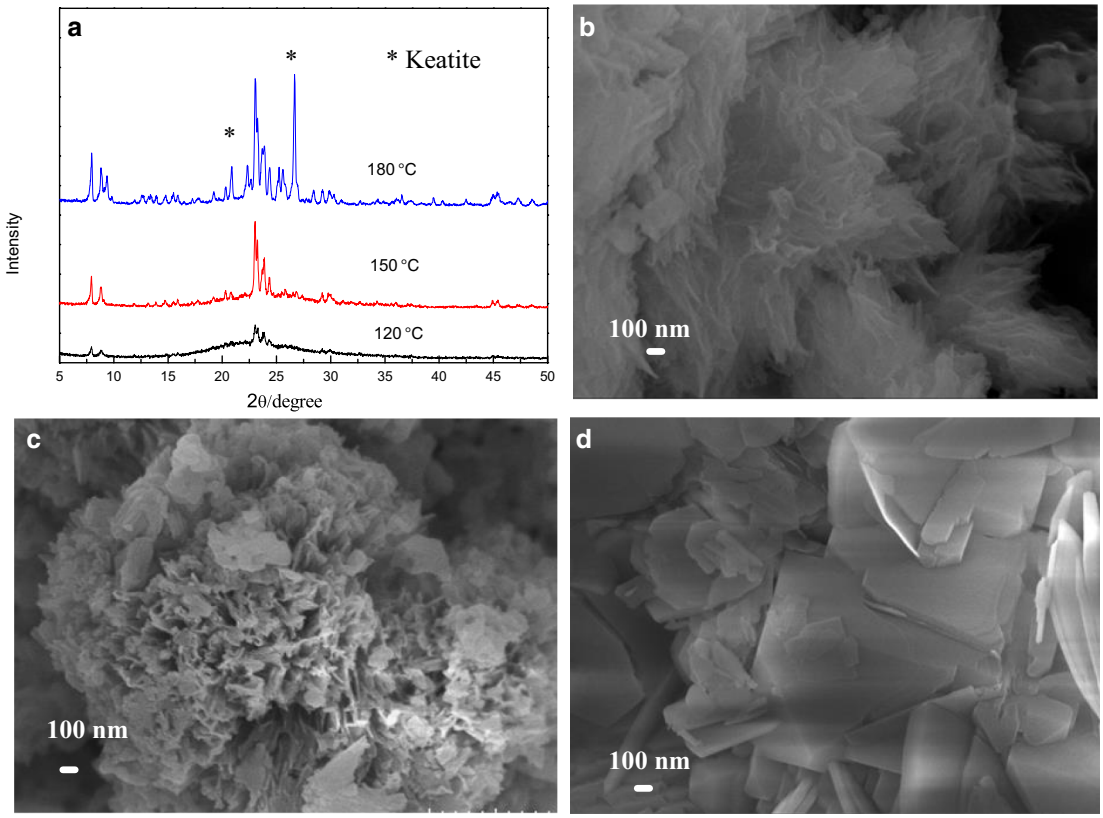

Fig. 5 XRD patterns (**a**) and SEM images of Hi-ZSM-5 synthesized at different temperature of 120 °C (**b**), 150 °C (**c**) and 180 °C (**d**). The initial gel composition was $60SiO_2$:$1Al_2O_3$:$4Na_2O$:6CTAB:$2400H_2O$ with 0.5 wt% with aging temperature 60 °C 24 h

the SEM images (Fig. 5b). In addition, the low-angle XRD pattern (Fig. S3) shows a clear signal for 2θ between 1.5° and 2.5°, which can be ascribed the short-range ordered mesoporous structure and this is a clear evidence of the formation amorphous lamellar mesoporous material. Furthermore, 421 $m^2\ g^{-1}$ of S_{BET} and 36 $m^2\ g^{-1}$ of S_{micro} for 120 °C (Tab. S1) also prove that at a low temperature, the solution energetics is only favorable for the formation of the amorphous mesophase. At 150 °C, the high quality of Hi-ZSM-5 zeolite was synthesized with agglomerations of nanosheet crystals. When the crystallization temperature was increased further to 180 °C, a mixture of bulk ZSM-5 and a dense phase (Keatite) with no mesopore structure was formed. According to Li et al., the long chain surfactants CTAB was decomposed to the short chain aklylammonium species which led to the formation of microporous materials, when the crystallization temperature exceeded 170 °C [31]. Therefore, a bulk ZSM-5 was formed instead of Hi-ZSM-5 at higher temperature 180 °C. The textural properties of the synthesized sample obtained at 180 °C with 241 $m^2\ g^{-1}$ of S_{BET} and 208 $m^2\ g^{-1}$ of S_{micro} are similar to C-ZSM-5, as shown in Tab. S1, which are consistent with the results of Fig. 5. The temperature 150 °C was found to be the optimal for CTAB to direct the formation of Hi-ZSM-5 in this work.

The synthesized samples after different times of synthesis were tracked using XRD, N_2 adsorption–desorption and SEM for studying the growth process of the Hi-ZSM-5, and the corresponding synthesis molar composition was $60SiO_2$:$1Al_2O_3$:$4Na_2O$:6CTAB:$2400H_2O$ with 0.5 wt% of the ZSM-5 seed crystals. The solids were designated as MZ-0.1-y d, in which 0.1 represents the molar ratio of CTAB to SiO_2, and y represents the crystallization time.

Figure 6 shows the XRD patterns corresponding to these materials obtained at different crystallization time. In the low-angle XRD patterns, a clear single peak at between 1.5° and 2.5° can be observed at 2 days (Fig. 6a), which implies that the mesoporous materials is firstly generated by the assistance of CTAB. As the crystallization time is extended, the peak of low-angle XRD weakens gradually and finally almost disappears after crystallization for 5 days. Meanwhile, only the negligible XRD peaks related to MFI phase can be detected after crystallization at 150 °C for 2 d, which is mainly due to the addition of seeds, implying its long-range molecular disorder, as shown in Fig. 6b. The XRD peaks of MFI phase become intensified by prolonging of crystallization time. Well crystallized ZSM-5 phase is formed after crystallization at 150 °C for 4 days. When further increasing the crystallization time to 5 days, the

crystallinity of ZSM-5 phase tends to decrease slightly. Meanwhile, some secondary phases such as Keatite and Mordenite appear. It indicates that time needed for the crystallization ZSM-5 phase is from 2 to 4 days, in case of longer crystallization time, the crystallization path is more likely to direct toward the formation of secondary undesired phases rather than ZSM-5.

The N_2 sorption isotherms and the relevant BJH pore size distributions of the solids crystallized with different time are given in Fig. 7. The texture properties of derived thereof are listed in Table 2. It shows that the sample crystallized for

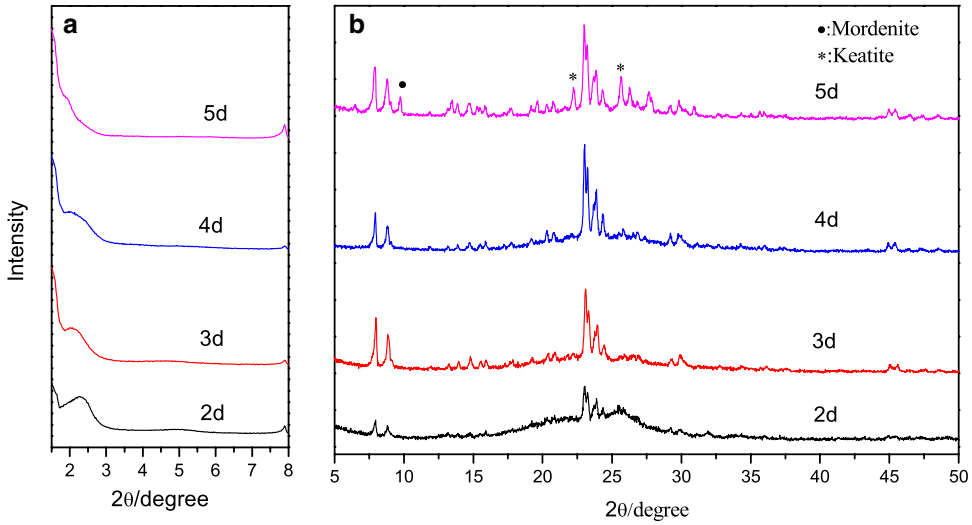

Fig. 6 Low-angle and wide-angle XRD patterns of the samples crystallization at 150 °C for 2 days, 3 days, 4 days, 5 days

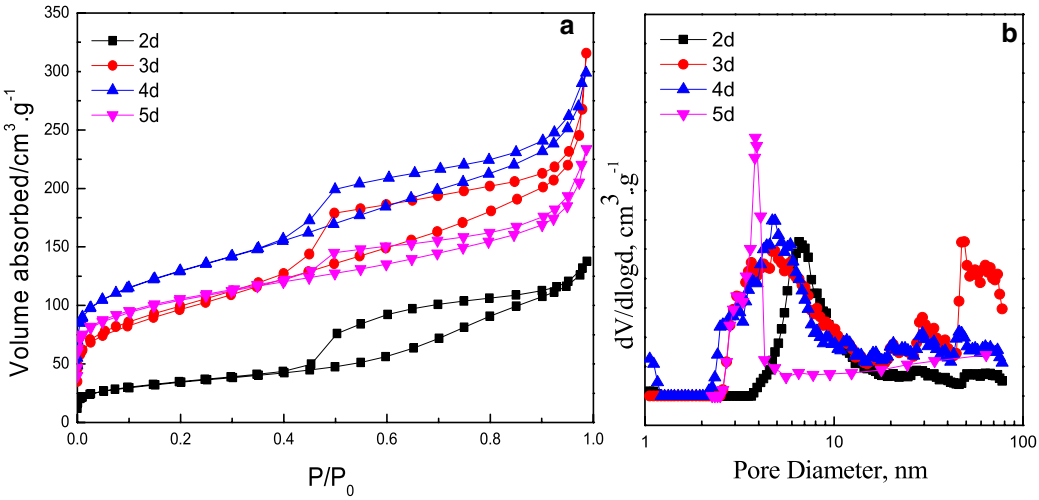

Fig. 7 Nitrogen adsorption–desorption isotherms and the corresponding BJH pore size distribution of the samples crystallization at 150 °C for 2 days, 3 days, 4 days, and 5 days

Table 2 Textural parameters of the samples crytallization at 150 °C for different periods

Sample	Specific surface area ($m^2\ g^{-1}$)			Pore volume ($cm^3\ g^{-1}$)		
	S_{BET}	S_{micro}	S_{ex}	V_{tot}	V_{micro}	V_{meso}
MZ-0.1-2d	113	0	113	0.2	0	0.2
MZ-0.1-3d	316	59	257	0.46	0.04	0.42
MZ-0.1-4d	444	157	286	0.45	0.08	0.37
MZ-0.1-5d	364	222	141	0.34	0.08	0.27

2 days exhibits typical IV isotherm with a hysteresis loop, a typical of uniform mesoporous material with mesopores around 7–9 nm. As shown in Table 2, the sample crystallized for 2 days has no micropores with an external surface area of 113 $m^2\ g^{-1}$ and a mesopore volume of 0.2 $cm^3\ g^{-1}$, which is also confirmed by the XRD characterization suggesting only formation of mesophases at an early stage. When the crystallization time increases to 3 d, the N_2 isotherms shows a larger adsorption at a higher P/P_0 and changes to combined features of types I and IV with a hysteresis loop. It indicates that substantial mesopores are developed and a certain amount of micropores ($S_{micro} = 59\ m^2\ g^{-1}$) are formed at the same time. The external surface area increases from 113 to 257 $m^2\ g^{-1}$ for MZ-0.1-3d. With the increase of crystallization time to 4d, MZ-0.1-4d shows a higher micropore surface area of 157 $m^2\ g^{-1}$, which corresponds to a higher microporous volume ($V_{micro} = 0.08\ cm^3\ g^{-1}$). It is due to formation of microporous structure, consistent with its good crystallinity. It also shows a little higher external surface area ($S_{ex} = 286\ m^2\ g^{-1}$) compared with MZ-0.1-3d. Further increasing the crystallization time to 5 days results in a slight increase of the micropore surface area and a dramatic decrease of external surface area. Furthermore, as the crystallization time increases from 3 to 5 days, the hysteresis loop narrows down indicating the formation of smaller mesopores.

The morphologies with different crystallization time are shown in Fig. 8. The solids crystallized for 2 days exhibits amorphous phase with lamellar-like morphologies. This is consistent with the XRD pattern and N_2 sorption results. The lamellar structure is becoming clearer and clearer while the amount of amorphous phases decreases after 3 days which may be due to the initial formation of crystalline ZSM-5 (The characteristic peaks attributable to the MFI topology can be investigated in the wide-angle XRD region at this stage). When the crystallization time is increased to 4 d, the products display a loosely nanosheet agglomerations while amorphous phase nearly disappears. Further prolonging the crystallization time to 5 days, it is found that the primary nanosheet crystals were closed stacked at an oriented direction and a small amount of impure dense phase can be investigated.

From the information discussed above, a possible formation process of the Hi-ZSM-5 zeolite was proposed in this work. The ZSM-5 seeds added in the initial gel were dissolved into subnanocrystals which induced the zeolite precursors into a large number of subnanocrystals by the proceeding of aging. When the mesoporogen CTAB was mixed with these subnanocrystals, mesoporous aluminosilicate structure with lamellar-like morphologies was firstly obtained. Then the nanocrystals arranged and a large number of micropores were formed in-situ during the hydrothermal synthesis process. Finally, the Hi-ZSM-5 zeolite instead of a mixture of zeolite and mesophase were formed due to the formation of subnanocrystals with high polymerization degree.

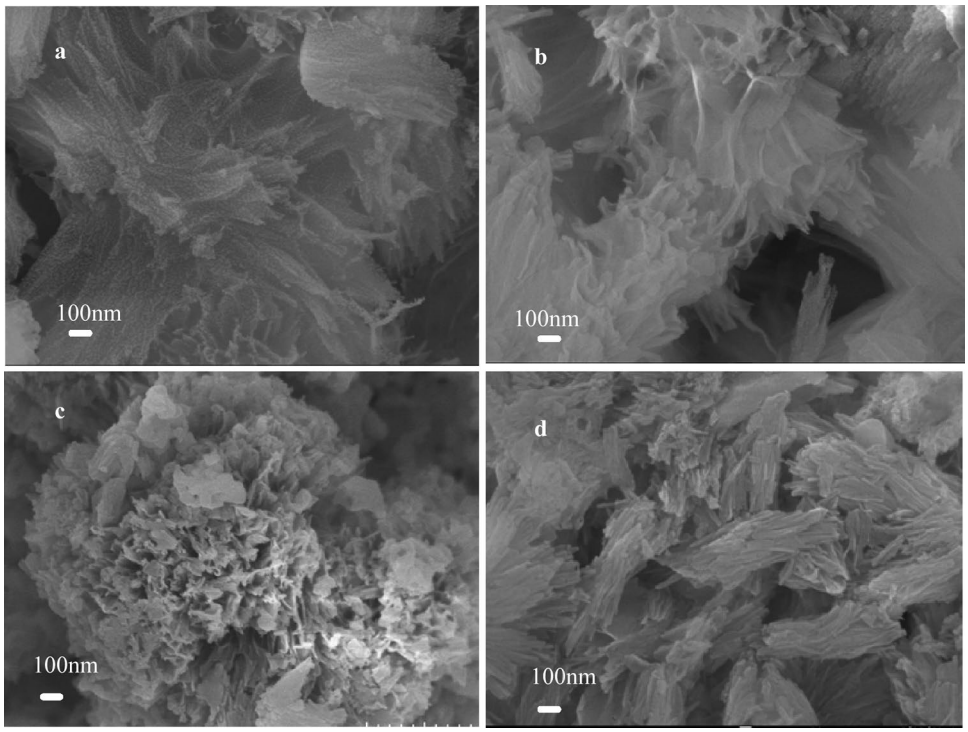

Fig. 8 SEM images of the samples crystallization at 150 °C for 2 days (**a**), 3 days (**b**), 4 days (**c**), and 5 days (**d**)

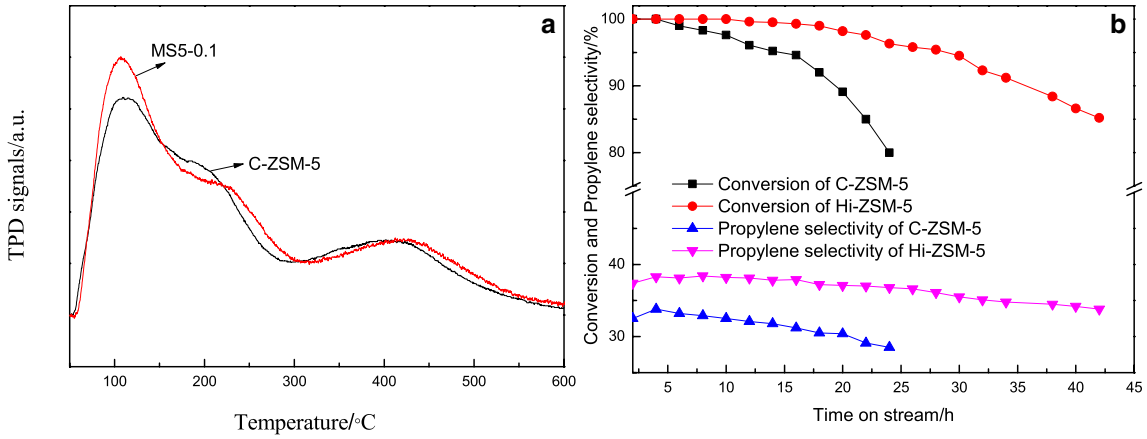

Fig. 9 NH_3-TPD profiles (**a**) and catalytic performance in MTP (**b**) of Hi-ZSM-5 and C-ZSM-5

3.3 Acidity and catalytic properties of Hi-ZSM-5

The acidity of catalyst significantly affects the catalytic performance. Figure 9 shows the NH_3-TPD curves of the MZ-0.1and C-ZSM-5 crystallized at 150 °C for 4 d, which have the same initial molar composition except CTAB. As shown in Fig. 9, two evident desorption peaks at 100–300 °C and 300–500 °C are observed for both samples, which assign to NH_3 desorption from weak acidic sites and strong acidic sites, respectively. It is clear that the two samples have the equal amounts of strong acid sites which is important for catalytic reaction [32]. The amounts of weak acid of MZ-0.1 are higher than that of C-ZSM-5 which may be due to the presence of more accessible Si–OH in the MZ-0.1 with larger external surface and abundant intercrystalline mesopores [33]. It is generally considered that the weak acid sites can control some side reactions such as hydrogen-transfer reaction [34].

It has been proved that the hierarchical zeolites are beneficial to large organic molecules reaction. The catalytic performances of the MZ-0.1 was tested for MTP reaction at 400 °C and the results are shown in Fig. 9b. We referred to the running time from the beginning to the methanol conversion decreasing to about 90% as the catalytic deactivation. From the methanol conversion versus time on stream (TOS), it can be observed that both Hi-ZSM-5 and C-ZSM-5 exhibit 100% methanol conversion initially, implying the initial high activity for Hi-ZSM-5 and C-ZSM-5. This is because the amounts of the strong acidic sites are nearly equal. While, methanol conversion of C-ZSM-5 drops blow 90% and then decreases dramatically after 17 h. It is due to the poor diffusion efficiency which led to quick coke deposition on the zeolite. Compared with the C-ZSM-5, Hi-ZSM-5′s longevity as catalyst is excellent, with a 34 h longer catalytic lifetime. The longer catalytic lifetime on Hi-ZSM-5 is attributed to the enhanced accessibility of active sites provided by the unique micro–mesoporous structure which improves mass transformation and thereby enhances the diffusion rate and suppresses coke formation at the pore mouths. The average product selectivities of the two zeolites during MTP reaction are comparable (Table S2). However, the shorter residence time of cracking intermediates in Hi-ZSM-5 makes it easier to diffuse out of the zeolite which leads to a higher propylene selectivity than that of C-ZSM-5 [35].

4 Conclusion

Hi-ZSM-5 zeolite was successfully synthesized by the self-assembly with nanocrystals by employing CTAB as mesoporogen without any organic amine as SDA. N_2 adsorption/desorption measurement demonstrated that the Hi-ZSM-5 possessed larger specific surface area and higher mesopore volume, in comparison with C-ZSM-5. SEM and TEM images showed that the Hi-ZSM-5 zeolite was flake-shaped agglomerations with regular intercrystal mesopores of 3–7 nm. Among the parameters studied, the ratio of CTAB/SiO_2, aging temperature, reaction temperature and reaction time had pronounced influence on the physicochemical properties of the synthesized samples. Synthesis process indicated that the ordered mesoporous phases were first formed with the assistance of CTAB and then crystallized through in-situ consumption of amorphous silica-alumina species to the Hi-ZSM-5. The induced a large number of subnanocrystals was the key to prevent the separation of mesophases and zeolite crystals. Compared with C-ZSM-5, the Hi-ZSM-5 had a higher stability and propylene selectivity which was proved by the methanol to propylene (MTP) reaction.

Acknowledgements This work is supported by the Project of Shandong Province Higher Educational Science and Technology Program (J18KB053).

Compliance with ethical standards

Conflict of interest The authors declare that they have no conflict of interest.

References

1. C. Martínez, A. Corma, Coordin. Chem. Rev. **255**, 1558–1580 (2011)
2. B. Qiu, F. Jiang, W. Lu, B. Yan, W. Li, Z. Zhao, A. Lu, J. Catal. **385**, 176–182 (2020)
3. Y. Sang, H. Li, J. Solid State Chem. **271**, 326–333 (2019)
4. L. Tosheva, V.P. Valtchev, Chem Mater. **17**, 2494–2513 (2005)
5. G.A. Tompsett, W.C. Conner, K.S. Yngvesson, Chem. Phys. Chem. **7**, 296–319 (2006)
6. C.T. Kresge, M.E. Leonowicz, W.J. Roth, Nature **359**, 710–714 (1992)
7. A.L. Figueiredo, A.S. Araujo, M. Linares, Á. Peral, R.A. García, D.P. Serrano, V.J. Fernandes Jr., J. Anal. Appl. Pyrol. **117**, 132–140 (2016)
8. J. Yu, J.L. Shi, H.R. Chen, J. Yan, D. Yan,Micropor. Mesopor. Mater. **46**, 153–162 (2001)
9. R. Sabarish, G. Unnikrishnan, J. Porous Mater. (2020). https://doi.org/10.1007/s10934-019-00852-5
10. A. Bolshakov, R. Poll, T. Bergen-Brenkman, S.C.C. Wiedemann, N. Kosinov, E.J.M. Hensen, Appl. Catal. B Environ. **263**, 1–10 (2020)
11. K. Zhang, Z. Liu, X. Yan, X. Hao, M. Wang, C. Li, H. Xi, Langmuir **33**, 14396–14404 (2017)
12. M.S.M. Kamil, K.K. Cheralathan, J Porous Mat (2020). https://doi.org/10.1007/s10934-019-00839-2
13. G.T. Neumann, J.C. Hicks, Cryst. Growth. Des. **13**, 1535–1542 (2013)
14. Y. Wang, K. Liu, T. He, J. Wu, Y. Fang, J. Solid State Chem. **194**, 416–421 (2012)
15. A. Feng, Y. Yu, L. Mi, Y. Cao, Y. Yu, L. Song, Micropor. Mesopor. Mater. **280**, 211–218 (2019)
16. Y. Jiao, L. Forster, S. Xu, H. Chen, J. Han, X. Liu, Y. Zhou, J. Liu, J. Zhang, J. Yu, C.D. Agostino, X. Fan, Angew. Chem. **132**, 2–11 (2020)
17. Y.S. Tao, H. Kanoh, K. Kaneko, J. Phys. Chem .**107**, 10974–10976 (2003)
18. F.J. Liu, T. Willhammar, L. Wang, L. Zhu, Q. Sun, X. Meng, W. Cabrera, X. Zou, F. Xiao, J. Am. Chem. Soc. **134**, 4557–4560 (2012)
19. R. Barakov, N. Shcherban, P. Yaremov, I. Bezverkhyy, A. Baranchikov, V. Trachevskii, V. Tsyrina, V. Ilyin, Micropor. Mesopor. Mater. **237**, 90–107 (2017)
20. M. Choi, K. Na, J. Kim, Y. Sakamoto, O. Terasaki, R. Ryoo, Nature **461**, 246–249 (2009)
21. D. Xu, Y. Ma, Z. Jing, L. Han, B. Singh, J. Feng, X. Shen, F. Cao, P. Oleynikov, H. Sun, O. Terasaki, S. Che, Nat. Commun. **4262**, 1–9 (2014)
22. K. Zhang, C. Li, Z. Liu, M. Wang, X. Yan, H. Xi, Chem. Asian J. **20**, 2711–2719 (2017)
23. Y. Liu, W. Zhang, T.J. Pinnavaia, Angew. Chem. Int. Ed. **40**, 1255–1258 (2001)
24. K.S. Triantafyllidis, E.F. Iliopoulo, E.V. Antonakou, A. Lappas, H. Wang, T. Pinnavaiac, J. Micropor. Mesopor. Mater. **99**, 132–139 (2007)
25. M. Liu, J. Li, W. Jia, M. Qin, Y. Wang, K. Tong, H. Chen, Z. Zhu, RSC Adv. **5**, 9237–9240 (2015)
26. Y. Zhu, Z. Hua, J. Zhou, L. Wang, J. Zhao, Y. Gong, W. Wu, M. Ruan, J.L. Sh, Chem. Eur. **17**, 14618–14627 (2011)
27. M.L. Goncalves, L.D. Dimitrov, M.H. Jordao, M. Wallau, E.A. Urquieta-Gonzalez, Catal. Today **133–135**, 69–79 (2008)
28. T. Xue, H. Liu, Y. Zhang, H. Wu, P. Wu, M. He, Micropor. Mesopor. Mater. **242**, 190–199 (2017)
29. H. Chen, Y. Wang, F. Meng, C. Sun, H. Li, Z. Wang, F. Gao, X. Wang, S. Wang, Micropor. Mesopor. Mater. **244**, 301–309 (2017)
30. L. Meng, B. Mezari, M.G. Goesten, E.J.M. Hensen, Chem. Mater. **29**, 4091–4096 (2017)
31. L. Huang, X. Chen, Q. Li, J Mater. Chem. **11**, 610–615 (2001)
32. Q. Yu, X. Meng, J. Liu, C. Li, Q. Cui, Micropor. Mesopor. Mater. **181**, 192–200 (2013)
33. N. Katada, Y. Kageyama, M. Niwa, J. Phys. Chem. B **104**, 7561–7564 (2000)
34. M. Rostamizadeh, A. Taeb, J. Ind. Eng. Chem. **27**, 297–306 (2015)
35. C. Mei, P. Wen, Z. Liu, H. Liu, Y. Wang, W. Yang, Z. Xie, W. Hua, Z. Gao, J. Catal. **258**, 243–249 (2008)